International Journal of Computational Science and Engineering

ISSN online: 1742-7193 - ISSN print: 1742-7185
https://www.inderscience.com/ijcse

An improved blind/referenceless image spatial quality evaluator algorithm for image quality assessment

Xuesong Li, Jinfeng Pan, Jianrun Shang, Alireza Souri, Mingliang Gao

DOI: 10.1504/IJCSE.2022.10051266

Article History:

Received:	21 May 2022
Last revised:	21 June 2022
Accepted:	25 July 2022
Published online:	25 January 2024

An improved blind/referenceless image spatial quality evaluator algorithm for image quality assessment

Xuesong Li, Jinfeng Pan* and Jianrun Shang

School of Electrical and Electronic Engineering,
Shandong University of Technology,
Zibo, Shandong, China
Email: sdut_lxs@163.com
Email: pjfbysj@163.com
Email: jianrun_shang@163.com
*Corresponding author

Alireza Souri

Department of Computer Engineering,
Haliç University,
Istanbul, Turkey
Email: alirezasouri.research@gmail.com

Mingliang Gao

School of Electrical and Electronic Engineering,
Shandong University of Technology,
Zibo, Shandong, China
Email: sdut_mlgao@163.com

Abstract: Image quality assessment (IQA) methods are generally studied in the spatial or transform domain. Due to the BRISQUE algorithm evaluating the quality of an image only based on its natural scene statistics of the spatial domain, the frequency features that are extracted from the modulation transfer function (MTF) are applied to improve its performance. MTF is estimated based on the slanted-edge method. The two-dimensional grey fitting algorithm is utilised to estimate the edge slope more accurately. Then the three-order Fermi function is utilised to match the preliminary estimated edge spread function to reduce the aliasing influence on MTF estimation. The features such as crucial frequency and the MTF value at Nyquist frequency are calculated and adopted to the BRISQUE method to assess the image quality. Experimental results on the image quality assessment databases illustrated that the proposed method outperforms the BRISQUE method and some other common methods, based on the linear and nonlinear correlation between the image quality assessed by the methods and their subjective value.

Keywords: image quality assessment; IQA; modulation transfer function; MTF; Fermi function; feature extraction.

Reference to this paper should be made as follows: Li, X., Pan, J., Shang, J., Souri, A. and Gao, M. (2024) 'An improved blind/referenceless image spatial quality evaluator algorithm for image quality assessment', *Int. J. Computational Science and Engineering*, Vol. 27, No. 1, pp.48–56.

Biographical notes: Xuesong Li is pursuing his MS at the School of Electrical and Electronic Engineering, Shandong University of Technology, Zibo, China. His research interests include image processing and pattern recognition.

Jinfeng Pan received her PhD in Singal and Information Processing at the University of Chinese Academy of Sciences, Xian, China, in 2016. From 2005, she has worked in the School of Electrical and Electronic Information Engineering, Shandong University of Technology, Zibo, China. Her main research interests include image denoising, assessment and deep learning.

Jianrun Shang is pursuing his MS at the School of Electrical and Electronic Engineering, Shandong University of Technology, Zibo, China. His research interests include image processing and machine learning.

Alireza Souri received his BS in Software Engineering from University College of Nabi Akram, Iran, and his MSc and PhD in Software Engineering from the Science and Research Branch, Islamic Azad University, Iran. He is a researcher and Lecturer at the Islamic Azad University. Up to now, he has authored/co-authored 30 academic articles. He served on the program committees and the technical reviewer of several ISI-index journals and international conferences. His research interests include formal specification and verification, model checking, grid and cloud computing, IoT and social networks.

Mingliang Gao received his PhD in Communication and Information Systems from the Sichuan University, Chengdu, China, in 2013. From 2018 to 2019, he was a Visiting Scholar with the School of Engineering, The University of British Columbia, Okanagan. He is currently an Associate Professor with the School of Electrical and Electronic Engineering, Shandong University of Technology, Zibo, China. His main research interests include image fusion and deep learning.

1 Introduction

Image quality could validate the performance of both the image capture devices and the algorithms that tackle various kinds of image processing problems. Many types of research aim to improve and utilise the quality of images, e.g., image fusion (Tambe et al., 2021; Wei et al., 2021), noise quantisation (Yu et al., 2022), image denoising (Laksir et al., 2019), palm-print recognition (Poonia and Ajmera, 2022). Image quality assessment (IQA) algorithms are powerful tools to judge the image quality. Full-reference methods and no-reference methods are generally used IQA methods. Full-reference image quality measurement methods are widely used for the simple computational process and good performance. Peak signal-to-noise ratio (PSNR), structure similarity index (SSIM) (Wang et al., 2004), multiscale structure similarity index (MS-SSIM) (Wang et al., 2003) and some deep learning-based IQA methods (Zhou and Chen, 2021; Saeed et al., 2021; Zhou et al., 2021) are all pertain to full-reference IQA method.

No-reference (NR) IQA method may be more convenient if the original reference image is unknown. Some NR IQA algorithms evaluate the quality of an image using features extracted from the transform domain. The blind image quality index (BIQI) (Moorthy and Bovik, 2010) assesses the quality of an image using the features related to the wavelet coefficients. BLIINDS-II (Saad et al., 2012) extracts the features of the distribution of discrete cosine transform (DCT) coefficients to compute the image quality. The distortion identification-based image verity and integrity evaluation (DIIVINE) algorithm (Moorthy and Bovik, 2011) utilises the wavelet coefficients of an image to predict its quality. Another kind of NR IQA methods evaluate the quality of an image using features related to image spatial characteristic, Blind/referenceless image spatial quality evaluator (BRISQUE) (Mittal et al., 2012b) assesses the image quality by its spatial statistical characteristics. The third kind NR IQA algorithm combines the features both in spatial and transform domain, stereoscopic IQA (Guan et al., 2022) utilising features related to complex contourlet coefficients and spatial characteristics of an image. Spatial-spectral entropy-based quality (SSEQ) (Liu et al., 2014) uses spatial and frequency entropies to assess the image quality. The quality of the super-resolution image is also measured by both the spatial and frequency characteristic (Zhou et al., 2019).

Only using spatial features, BRISQUE lacks the frequency analysis of an image. It might be helpful to add some frequency characteristics to BRISQUE in IQA. In this paper, we added the frequency features to BRISQUE to address this problem. The frequency features are extracted from the modulation transfer function (MTF) that is estimated using the image, MTF can represent both the quality of an image and the device that captures the image. After adding the frequency features, the proposed IQA method contains both the spatial and frequency characteristic of an image, which can improve the performance of IQA. MTF is the frequency response of an imaging system (Bundy and Wallen, 1986). It could be estimated by an image captured by the imaging system. Therefore, MTF can also denote the quality of the image, especially the quality that relates to its frequency characteristic. MTF is widely utilised in the image enhancement, such as the super-resolution reconstruction of remote sensing images (Fan et al., 2017). In this paper, we introduce the frequency information to the BRISQUE method to improve its performance. Features extracted from MTF are utilised as the frequency characteristics supplement for BRISQUE algorithm. Twelve characteristic parameters are extracted for image quality evaluation, i.e., crucial frequency, MTF values at zero and Nyquist frequency, and the average MTF values of every 0.1 cycle/pixel interval in the range of $[0, 0.8]$ cycles/pixel. The contributions of the proposed work mainly include two aspects, which can be described as,

1 To improve the performance of the MTF estimation, a two-dimensional grey fitting method is utilised to estimate the slope of the slanted-edge, followed by the edge spread function is fitted by three-order Fermi function. Using this method, the aliasing of the MTF is reduced.

2 We added 12 frequency features extracted from the MTF of an image to BRISQUE algorithm to improve the IQA performance.

The remaining sections are organised as follows. Section 2 presents the BRISQUE algorithm. Section 3 introduces the slanted-edge MTF estimation method and its improvement. The features extracted from MTF are also presented in this section. Section 4 illustrates the simulation results. Section 5 presents the discussion about the proposed method.

2 Blind/referenceless image spatial quality evaluator

Blind/referenceless image spatial quality evaluator (BRISQUE) (Mittal et al., 2012b) is a two-scale natural scene statistics IQA algorithm. It maps the spatial features of an image into the generalised Gaussian distribution (GGD) and the asymmetric GGD (AGGD) with different parameters on each scale. The parameters of the fitted distributions serve as the features to IQA. The spatial characteristic BRISQUE used is the mean subtracted contrast normalised (MSCN) coefficient, which is defined as,

$$\hat{S}_{ij} = \frac{S_{ij} - m_{ij}}{\sigma_{ij} + c}, \tag{1}$$

where S_{ij} is the pixel grey, and c is a small positive constant to ensure the numerator is not divided by zero. m_{ij} and σ_{ij} are the local mean and standard variance of the assessed image, respectively.

According to the fact that the statistical property varies from different kinds of image distortion, GGD is used to fit the distribution of MSCN coefficients. GGD is formulated by,

$$g(z;\omega,\sigma^2) = \frac{\omega}{2\zeta\Gamma(1/\omega)} \exp\left(-\left(\frac{|z|}{\zeta}\right)^{\omega}\right), \tag{2}$$

where

$$\zeta = \sigma\sqrt{\frac{\Gamma(1/\omega)}{\Gamma(3/\omega)}}. \tag{3}$$

Here, $\Gamma(\cdot)$ is the gamma function. ω is a shape control parameter and σ^2 represents the variance. In each scale of BRISQUE, both ω and σ are used as quality assessment features.

BRISQUE models the statistical relationships of neighbouring MSCN coefficients of each of the four directions (horizontal, vertical, main-diagonal, and secondary diagonal) by AGGD, respectively,

$$g(z;h,\sigma_l^2,\sigma_r^2) = \begin{cases} \frac{h}{(\zeta_l+\zeta_r)\Gamma(1/h)exp\left(-(z/\zeta_l)^h\right)}, x<0 \\ \frac{h}{(\zeta_l+\zeta_r)\Gamma(1/h)exp\left(-(z/\zeta_r)^h\right)}, x>0 \end{cases} \tag{4}$$

$$\zeta_{l,r} = \sigma_{l,r}\sqrt{\frac{\Gamma(1/v)}{\Gamma(3/v)}}, \tag{5}$$

where h is the shape parameter and σ_l^2, σ_r^2 are spread parameters. These three parameters are also used as features of each scale of BRISQUE algorithm.

The last feature extracted from the AGGD model is θ, which is defined as,

$$\theta = (\zeta_r - \zeta_l)\frac{\Gamma(2/h)}{\Gamma(2/h)}. \tag{6}$$

The features (h, σ_l^2, σ_r^2, θ) extracted from each of the four directions constitute 16 features extracted from AGGD model in each scale. Adding the two features (ω, σ^2) extracted from GGD in each scale, BRISQUE extracts 18 features in each scale. Thus, BRISQUE extracts 36 features in two scales.

3 Improvement of MTF and its utilisation in the IQA

3.1 Slanted-edge MTF estimation and its improvement

ISO 12233 standard adopts a slanted-edge method to estimate the MTF (Estribeau and Magnan, 2004). This slanted-edge MTF estimation method is widely accepted. It estimates MTF by a region of interest (ROI) that contains a slanted-edge cropped from the studied image. Estimated by the ROI of the tested image, MTF could also represent the quality of the image and be helpful in assessing the image quality. One of its realisation methods is completed by Burns and Williams (2002). The MTF is estimated using the following steps. First, the derivative of the luminance of pixels in every row of the selected ROI is calculated. Then, the centroid of the derivative of every row is computed. After that, the centroids are used to estimate the slope of the line to perform a line fit on the slanted-edge. Using the slanted-edge method, the deviation of the evaluated slope of the slanted-edge is less than 0.5 degrees for many digital cameras (Burns, 2002). The edge spread function (ESF) is obtained by projecting the luminance of the pixels along the direction of the fitted line to the horizontal axis. The derivative of the ESF is the line spread function (LSF) of the image. MTF can be easily estimated because it is the Fourier transform of LSF.

To conquer the MTF estimation degradation caused by the error of edge slope, Zhang et al. (2018) proposed to skip the edge angle estimation. The method directly calculates the LSF of each row and its differential operation. However, most MTF estimation methods are still based on Burns' method. Williams (1998) studied the influences of several factors that affect the MTF estimation, including edge angle, noise, binning ratio, and the edge region clipped by different rows and columns of an image. Besides the noise and edge angle, Xie et al. (2018a) conducted a statistical analysis of the error of the MTF estimation. Alaruri (2016) measured the MTF by slanted-edge method using images captured by different illumination levels and concluded that better MTF estimation can be obtained at a higher illumination level. Much work has been done to improve the accuracy of slanted-edge MTF estimation method. Xie et al. (2018b) utilised the Tikhonov regularisation method to suppress the influence of noise in the ESF estimation.

To alleviate the influence of the noises on the ESF estimation, Tzannes and Mooney (1995) utilised a

third-order Fermi function to fit the ESF estimated by Burns' method. The third-order Fermi function is defined as,

$$F(x) = \sum_{i=1}^{3} \frac{a_i}{1 + e^{(x-b_i)/c_i}} + D, \tag{7}$$

where D is the minimum value of the ESF estimated by Burns' method. For each $i\,(i = 1, 2, 3)$, the unknown parameters a_i, b_i, and c_i denote the amplitude, centre, and an adjusting parameter for one Fermi function, respectively. Optimisation methods such as simplex minimisation can be used to find the optimal value of the three parameters. Their initial values are also determined by the ESF estimated by Burns' slanted-edge method. The details of which are described by Tzannes and Mooney (1995).

However, the slanted-edge might not be genuinely straight due to the noise or other image degradation factor, which would decrease the estimating precision of the slanted-edge slope. Masaoka (2018) proposed an MTF estimation method that can process a slanted-edge with any angle. The algorithm fits a two-dimensional function to the pixel illuminance of the ROI, which is represented by,

$$G_{fit}(i, j) = (G_H - G_L)C(i, m + j/k, \sigma) + G_L, \tag{8}$$

where $G_{fit}(i, j)$ is the fitted pixel grey value. G_H and G_L are the mean value of the high and low luminance of the slanted-edge ROI, respectively. $C(\cdot)$ is the cumulative distribution function of a Gaussian distribution with a standard variance σ that is set to be a constant in the experiment. The unknown slope k of the slanted-edge is estimated simultaneously with the mean m of the Gaussian distribution, using the nonlinear programming method.

Figure 1 From left to right, the DMOS of each image is 62.90, 0, 42.02, and 43.72, respectively

Figure 2 The selected slanted-edge ROI of each image in Figure 1

Inspired by the method of Masaoka (2018), we adopt the grey value fitted method to estimate the slanted-edge slope. Then, the pixels are projected along the edge direction to estimate the preliminary ESF, which is fitted by the third-order Fermi function to obtain the final ESF evaluation value. This third-order Fermi function fitted ESF (FESF) could obtain a smooth ESF. The MTF estimated by FESF is named FMTF in this paper.

Figure 3 Estimated ESF of each image in Figure 1 (see online version for colours)

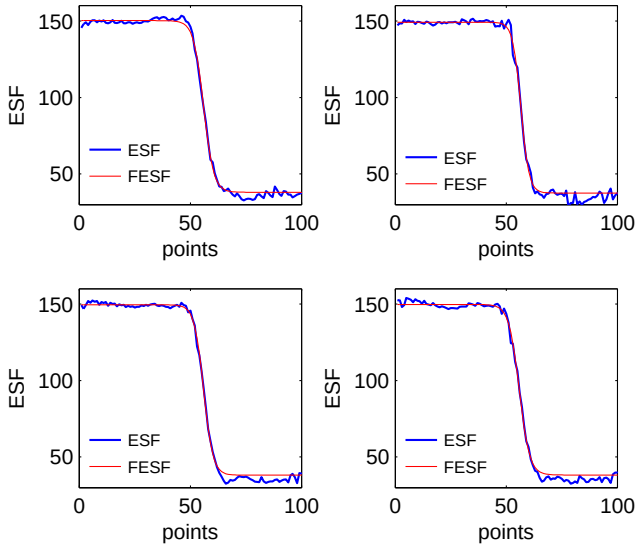

Figure 4 Estimated MTF of each image in Figure 1 (see online version for colours)

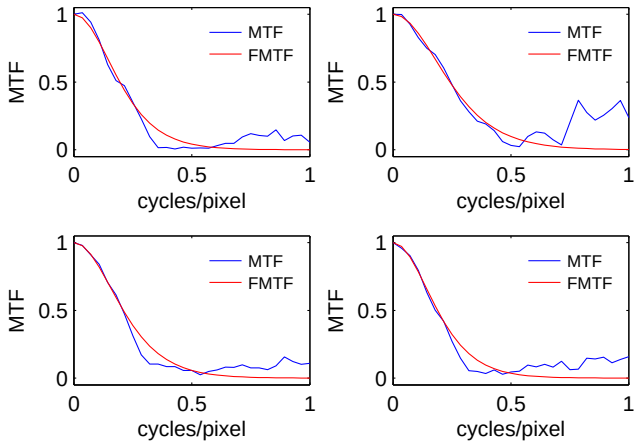

Figure 1 exhibits four different images selected from LIVE IQA database (Sheikh et al., 2006). From left to right, the difference mean opinion scores (DMOS) of the four images are 62.90, 0, 42.02, and 43.72, respectively. The larger the DMOS scores, the poorer the image quality is. Figure 2 is the corresponding slanted-edge ROI selected from the four images in Figure 1. The corresponding estimated ESFs of the images in Figure 1 are shown in Figure 3. It can be seen that compared with the ESF estimated by Burns' method (blue line), the curve of FESF (solid line) is smoother. As shown in Figure 4, there is no aliasing for the MTF evaluated by the proposed method. In reality, both the high and low grey level regions of the selected slanted-edge ROI might not have uniform pixel grey values. This deficiency would lead to the aliasing of the MTF, making the MTF not coincide with the quality of the image. The estimated

MTF of the reference image (DMOS= 0) is shown in the upper right of Figure 4. It can be seen that the aliasing of the slanted-edge method estimated MTF is higher than that of the other three images, which is inconsistent with the image quality. Meanwhile, the aliasing of the proposed FMTF decreases.

3.2 Feature parameters extracted from MTF

Figures 5 and 6 present some detailed results of selected slanted-edge ROI. The top row of Figures 5 and 6 marks the ROI selection of each tested image with a red rectangle. The details of the selected ROI are shown in the bottom row of Figures 5 and 6. The selected slanted edges are affected by noise, blurring, and other image degradations.

Figure 5 Example 1 for ROI selection of images

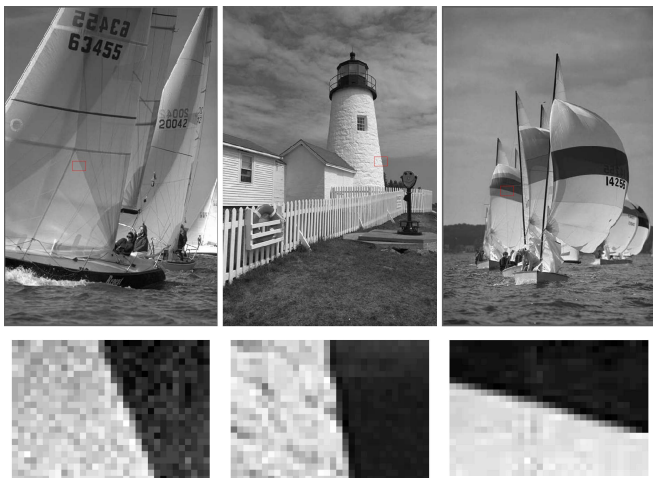

Note: The top row marked the selected ROI of each image with the red rectangle. The bottom row is the corresponding slanted-edge ROI.

Figure 6 Example 2 for ROI selection of images (see online version for colours)

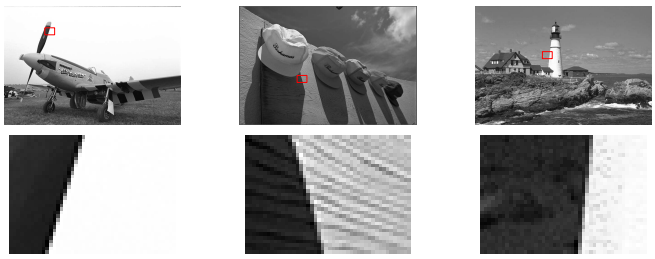

Note: The top row marked the selected ROI of each image with the red rectangle. the bottom row is the corresponding slanted-edge ROI.

MTF measures the spatial frequency resolution of an imaging device. It represents the frequency response of the image when estimated by the slanted-edge-based methods. Theoretically, the maximum value of MTF is 1, and MTF should acquire this maximum value when the frequency is equal to 0, i.e., $\mathrm{MTF}(0) = 1$ is the maximum. Since the ROI captured from images might not have the unchangeable greyscale on either side of the slanted-edge, the maximum value of the estimated MTF might not be at zero frequency. Figure 7 shows the estimated MTF of a JPEG distortion image from LIVE database. The maximum value of MTF estimated by Burns' method is 1.1 at the frequency of 0.06 cycles/pixel. In this paper, the MTF is normalised, which may cause $\mathrm{MTF}(0) \neq 1$. Since this property is important for MTF, we take $\mathrm{MTF}(0)$ as the first MTF feature in the quality assessment.

The second MTF feature we used is $\mathrm{MTF}(0.5)$. Because the sampling interval of the image is one pixel, the Nyquist frequency is 0.5 cycles/pixel (Burns and Williams, 2008). Hence, $\mathrm{MTF}(0.5)$ denotes the MTF at the Nyquist frequency, and it is significant in the IQA.

Figure 7 MTF of a JPEG image (see online version for colours)

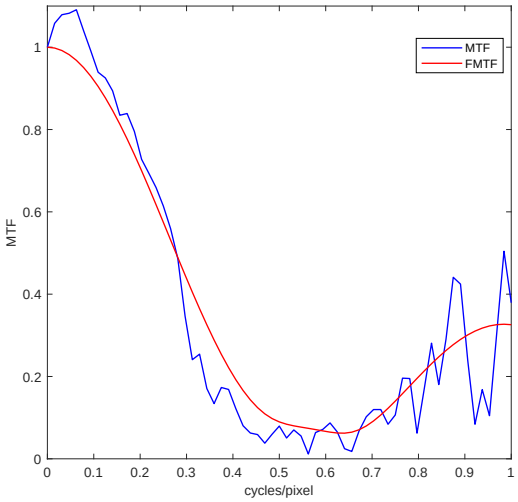

When estimating the ESF, the slanted-edge method interpolates the pixels of the slanted-edge ROI before they are projected to the horizontal axis, to reduce the aliasing of the estimated MTF. However, the aliasing is difficult to be eliminated. Thus, MTF at frequency 0.8 cycles/pixel, which is located among the frequency $[0.5, 1]$, is selected as the third MTF feature to measure the aliasing of the MTF.

The selected fourth MTF feature is related to the limiting visual resolution (Burns and Williams, 2008) of human beings. The MTF value of 0.1 is critical as it represents the limiting resolution of human vision. Therefore, the frequency at which MTF drops to 0.1 serves as the fourth MTF feature.

The last 8 extracted MTF features are the average MTF values of every 0.1 cycles/pixel interval in $[0, 0.8]$ cycles/pixel. When the frequencies are larger than 0.5 cycles/pixel, the mean MTF values can be used to judge the aliasing of the estimated MTF. The mean MTF values at smaller frequencies are important to the evaluation of image quality intuitively.

As described above, totally 12 features are extracted from the MTF of an image. Adding the 36 features extracted from BRISQUE algorithm, the proposed method uses 48 features to assess the quality of an image. The features include spatial and frequency characteristics

that derived from BRISQUE and MTF respectively. The proposed 12 features extracted from the MTF estimated by slanted-edge method combined with the features of BRISQUE constructs the novel IQA method, namely Slanted-Edge MTF BRISQUE (SEM-BRISQUE). Similarly, the 12 features extracted from the FMTF combined with the features of BRISQUE constructs another IQA method, named FSEM-BRISQUE.

Table 1 Mean PCC for 300 times train and test on the LIVE database

Method	*JP2K*	*JPEG*	*GBLUR*	*FF*	*Total*
BLIINDS-II	0.8988	0.9590	0.9033	0.8739	0.8592
NIQE	0.8678	0.7912	0.9403	0.7699	0.7821
PSNR	0.9027	0.9184	0.8193	0.8722	0.8597
SSIM	0.9372	0.9015	0.9432	0.9360	0.9059
MS-SSIM	0.9198	0.8736	0.8941	0.8942	0.8559
BRISQUE	0.9397	0.8853	0.9551	0.9055	0.9072
SEM-BRISQUE	*0.9547*	0.9309	0.9604	0.9113	0.9370
FSEM-BRISQUE	0.9517	*0.9414*	*0.9655*	*0.9528*	*0.9440*

Note: The ratio of trained and tested images is 3:1. The best results are highlighted in ital.

Table 2 Mean SROCC for 300 times train and test on the LIVE database

Method	*JP2K*	*JPEG*	*GBLUR*	*FF*	*Total*
BLIINDS-II	0.8691	0.9059	0.8509	0.7993	0.8194
NIQE	0.8908	0.8665	0.9381	0.8127	0.8578
PSNR	0.8798	0.9077	0.7899	0.8070	0.8432
SSIM	0.9247	*0.9297*	0.9271	*0.9389*	0.9347
MS-SSIM	0.9060	0.9279	0.8725	0.8991	0.9089
BRISQUE	0.9485	0.9138	0.9603	0.9278	0.9418
SEM-BRISQUE	0.9537	0.9087	0.9581	0.9323	0.9437
FSEM-BRISQUE	*0.9538*	0.9172	*0.9614*	0.9282	*0.9471*

Note: The ratio of trained and tested images is 3:1. The best results are highlighted in ital.

Table 3 Average PCC for 1,000 times train and test on the LIVE database

Method	*JP2K*	*JPEG*	*GBLUR*	*FF*	*Total*
BLIINDS-II	0.8592	0.9339	0.8606	0.7859	0.8146
NIQE	0.8666	0.7927	0.9390	0.7689	0.7821
PSNR	0.8996	0.9178	0.8299	0.8790	0.8617
SSIM	0.9357	0.9009	0.9437	*0.9351*	0.9059
MS-SSIM	0.9191	0.8714	0.8966	0.8945	0.8559
BRISQUE	0.9367	0.8853	0.9556	0.9096	0.9065
SEM-BRISQUE	*0.9531*	0.9314	0.9610	0.9097	0.9366
FSEM-BRISQUE	0.9503	*0.9424*	*0.9662*	0.9258	*0.9440*

Note: The ratio of trained and tested images is 3:1. The best results are highlighted in ital.

Table 4 Average SROCC for 1,000 times train and test on the LIVE database

Method	*JP2K*	*JPEG*	*GBLUR*	*FF*	*Total*
BLIINDS-II	0.8669	0.9077	0.8586	0.8067	0.8185
NIQE	0.8922	0.8730	0.9385	0.8087	0.8575
PSNR	0.8758	0.9077	0.8065	0.8174	0.8538
SSIM	0.9255	*0.9344*	0.9299	0.9404	0.9307
MS-SSIM	0.9100	0.9303	0.8814	0.9027	0.9089
BRISQUE	0.9306	0.9273	*0.9596*	0.9211	0.9361
SEM-BRISQUE	*0.9549*	0.9121	0.9593	*0.9304*	0.9440
FSEM-BRISQUE	0.9535	0.9204	0.9593	0.9297	*0.9477*

Note: The ratio of trained and tested images is 3:1. The best results are highlighted in ital.

4 Experimental results

We select 233 images from LIVE database to evaluate the performance of the two proposed IQA methods. In the experiments, the images are classified randomly into two non-overlapping sets, namely training set and test set. Using the images in the training set, a quality assessment model is trained by the support vector machine (Schölkopf et al., 2000). This model is used to evaluate the image quality in the test set.

The performance of the compared methods is appraised using linear Pearson's correlation coefficient metric (PCC) and the nonlinear Spearman's rank ordered correlation coefficient (SROCC) metric. Both PCC and SROCC can denote the resemblance between image scores predicted by the IQA method and the subjective DMOS values.

To illustrate the effectiveness of the two proposed methods, we choose six state-of-the-art methods that are based on the image spatial or frequency characteristic assessment for comparison, including PSNR, SSIM (Wang et al., 2004), MS-SSIM (Wang et al., 2003), BRISQUE (Mittal et al., 2012b), BLIINDS-II (Saad et al., 2012), and NIQE (Mittal et al., 2012a). The estimated image quality scores of the eight compared methods are adjusted by a logistic function (Sheikh et al., 2006) before computing the PCC and SROCC with DMOS.

The experiments are performed on the image sets of four different distortion types from LIVE database, namely JPEG2000 (JP2K), JPEG, Gaussian blur (GBLUR), and Fast fading (FF). In the first experiment, the training and test image set are randomly selected with a trained and tested image ratio of 3:1. The training and test experiment was repeated 300 times. Table 1 shows the results of average PCC values of the compared methods, in which the highest value of each image type is marked in ital. The average PCC values between DMOS and the image quality estimated by the compared methods for all the tested images are also computed, which is listed in the last column of Table 1, named total. In other tables of the paper, total also indicates the mean PCC or SROCC value of all the test images. It can be concluded from Table 1 that the proposed FSEM-BRISQUE method performs better than other methods, except for JP2K images. Compared with the BRISQUE method, the two proposed methods both obtain improvements on each distorted image type in terms of average PCC. The mean SROCC performance of this experiment is tabulated in Table 2, in which the best performance for each image type is also in ital. The proposed FSEM-BRISQUE ranks the first place in average SROCC value for all the tested images. Besides, it outperforms the compared methods on JP2K and GBLUR distorted images.

To check the influence of the train and test times, 1,000 times train and test examinations are implemented in the second experiment. The ratio of the trained and tested images is also set as 3:1. The experimental results of average PCC are shown in Table 3. It can be seen that, compared with BRISQUE, both the proposed methods obtain a higher average PCC for all the images. FSEM-BRISQUE method obtains the highest correlation with DMOS for the average of all the tested images, and its performances on JPEG and GBLUR images are better than the other methods. The SEM-BRISQUE method performs best on JP2K images. The average SROCC results shown in Table 4 indicate that the SEM-BRISQUE method achieves the highest SROCC value for the JP2K and FF images. FSEM-BRISQUE method outperforms the compared methods on the average SROCC of all the images. The two proposed methods both perform better than BRISQUE according to the average SROCC value for all the images. SEM-BRISQUE and FSEM-BRISQUE method do not outperform BRISQUE algorithm for JPEG and GBLUR images in terms of mean SROCC. The reason is that the estimated results are affected by the selected slanted-edge. If its quality is very different from that of the whole image, the estimation deviation will be high. As can be observed from Tables 1 to 4, the average PCC and SROCC results are almost the same for different test counts of 300 and 1,000.

Table 5 Average PCC for 1,000 times train and test on the LIVE database for all the images with different ratio of trained and tested images

Method	*Total (train and test ratio, 4:1)*	*Total (train and test ratio, 3:1)*
BLIINDS-II	0.8146	0.8146
NIQE	0.7821	0.7821
PSNR	0.8617	0.8617
SSIM	0.9059	0.9059
MS-SSIM	0.8559	0.8559
BRISQUE	0.9074	0.9065
SEM-BRISQUE	0.9389	0.9366
FSEM-BRISQUE	*0.9450*	*0.9440*

Note: The best results are highlighted in ital.

Table 6 Average SROCC for 1,000 times train and test on the LIVE database for all the images with different ratio of trained and tested images

Method	*Total (train and test ratio, 4:1)*	*Total (train and test ratio, 3:1)*
BLIINDS-II	0.8185	0.8185
NIQE	0.8575	0.8575
PSNR	0.8538	0.8538
SSIM	0.9347	0.9307
MS-SSIM	0.9089	0.9089
BRISQUE	0.9338	0.9361
SEM-BRISQUE	0.9451	0.9440
FSEM-BRISQUE	*0.9480*	*0.9477*

Note: The best results are highlighted in ital.

We supplemented the experiments, in which the trained and tested images are selected randomly by the ratio of 4:1. Also, 1,000 times train and test examinations are implemented. It can be observed from Tables 5 and 6 that compared with the results of trained and tested image

ratio of 3:1, the performance of SEM-BRISQUE and FSEM-BRISQUE methods are improved in terms both of the PCC and SROCC metrics.

5 Conclusions

In this paper, for the image whose quality needs to be estimated, a two-dimensional pixel grey fitting method is utilised to estimate the angle of the slanted-edge located in it. Then after projecting the pixels along the edge direction and the preliminary ESF value was estimated, the ESF is fitted by the third-order Fermi function to improve the estimation performance of MTF. After the MTF is obtained, totally 12 features including crucial frequency and some other important values of MTF are extracted to improve the quality assessment performance of BRISQUE. The frequency features extracted from the slanted-edge estimation MTF and the improved slanted-edge estimation MTF combines the features of BRISQUE constructing the features of the two proposed IQA method. Experimental results show that in the metric of mean PCC, the two proposed methods both achieve better performance compared with BRISQUE. With different train and test times, FSEM-BRISQUE method always obtains the highest average PCC correlation with DMOS on JPEG and GBLUR images. FSEM-BRISQUE method also achieves the highest average PCC for all the test images in different train and test ratios. SEM-BRISQUE method performs best for JP2K images. In the metric of SROCC, the proposed SEM-BRISQUE and FSEM-BRISQUE method both perform better than BRISQUE algorithm with different train and test times and ratios, except for the JPEG and GBLUR images when the train and test times is 1,000 and the train and test ratio is 3:1. Both in the metric of SROCC and PCC, FSEM-BRISQUE method performs best for the average of all the test images. The drawback of the two proposed methods is that they cannot assess the quality of an image without a slanted-edge. Fortunately, the multidirectional MTF estimation method that can deal with any angle has been studied by the researchers. These methods can explore the images our methods can process, and we will study it in the future. We are also interested in the study of using our proposed methods to assess the quality of the images sampled and reconstructed by the theory of compressive sensing.

References

Alaruri, S.D. (2016) 'Calculating the modulation transfer function of an optical imaging system incorporating a digital camera from slanted-edge images captured under variable illumination levels: Fourier transforms application using MATLAB', *Optik*, Vol. 127, No. 15, pp.5820–5824.

Bundy, A. and Wallen, L. (1986) *Catalogue of Artificial Intelligence Tools*, 2nd ed., Springer, Berlin.

Burns, P.D. (2000) 'Slanted-edge MTF for digital camera and scanner analysis', *Society for Imaging Science and Technology: Image Processing, Image Quality, Image Capture, Systems Conference*, IS&T, pp.6–29.

Burns, P.D. and Williams, D. (2000) 'Refined slanted-edge measurement for practical camera and scanner testing', (2002) *Society for Imaging Science and Technology: Image Processing, Image Quality, Image Capture, Systems Conference*, IS&T, pp.191–195.

Burns, P.D. and Williams, D. (2008) 'Sampling efficiency in digital camera performance standards', *Proceedings of SPIE – The International Society for Optical Engineering*, SPIE, 680805.

Estribeau, M. and Magnan, P. (2004) 'Fast MTF measurement of CMOS imagers using ISO 12233 slanted-edge methodology', *Proceedings of SPIE – The International Society for Optical Engineering*, SPIE, Vol. 5251, pp.243–252.

Fan, C., Wu, C.Y., Li, G. and Ma, J. (2017) 'Projections onto convex sets super-resolution reconstruction based on point spread function estimation of low-resolution remote sensing images', *Sensors*, Vol. 17, No. 2, p.362.

Guan, T.X., Li, C.F., Zheng, Y.H., Zhao, S.H. and Wu, X.J. (2022) 'No-reference stereoscopic image quality assessment on both complex complex contourlet and spatial domain via kernel ELM', *Signal Processing: Image Communication*, Vol. 101, No. 116547.

Laksir, S., Chaoub, A. and Tamtaoui, A. (2019) 'Iterative algorithms for impulsive noise reduction in OFDM-based power line communications', *Inernational Journal of Embedded Systems*, Vol. 11, No. 2, pp.147–162.

Liu, L.X., Liu, B., Huang, H. and Bovik, A.C. (2014) 'No-reference image quality assessment based on spatial and spectral entropies', *Signal Processing: Image Communication*, Vol. 29, No. 8, pp.856–8634.

Masaoka, K. (2018) 'Accuracy and precision of edge-based modulation transfer function measurement for sampled imaging systems', *IEEE Access*, Vol. 6, No. 8412181, pp.41079–41086.

Mittal, A., Soundararajan, R. and Bovik, A.C. (2012a) 'Making a 'completely blind' image quality analyzer', *IEEE Signal Processing Letters*, Vol. 20, No. 3, pp.209–212.

Mittal, A., Moorthy, A.K. and Bovik, A.C. (2012b) 'No-reference image quality assessment in the spatial domain', *IEEE Transaction on Image Processing*, Vol. 21, No. 12, pp.4695–4708, IEEE.

Moorthy, A.K. and Bovik, A.C. (2010) 'A two-step framework for constructing blind image quality indices', *IEEE Signal Processing Letters*, Vol. 17, No. 5, pp.513–516.

Moorthy, A.K. and Bovik, A.C. (2011) 'Blind image quality assessment: from natural scene statistics to perceptual quality', *IEEE Transactions on Image Processing*, Vol. 20, No. 12, pp.3350–3364.

Poonia, P. and Ajmera, P.K. (2022) 'Palm-print recognition based on quality estimation and feature dimension', *International Journal of Computational Science and Engineering*, Vol. 25, No. 2, pp.116–127.

Saad, M., Bovik, A.C. and Charrier, C. (2012) 'Blind image quality assessment: a natural scene statistics approach in the DCT domain', *IEEE Transaction on Image Processing*, Vol. 21, No. 8, pp.3339–3352.

Saeed, S.U., Fu, Y.G., Baum, Z.M.C., Yang, Q.Y., Rusu, M., Richard, E., Fan, R.E., Sonn, G.A., Barratt, D.C. and Hu, Y.P. (2021) *Learning Image Quality Assessment by Reinforcing Task Amenable Data Selection*, arXiv Preprint, arXiv.

Schölkopf, B., Smola, A.J., Williamson, R.C. and Bartlett, P.L. (2000) 'New support vector algorithms', *Neural Computation*, Vol. 12, No. 5, pp.1207–1245.

Sheikh, H.R., Sabir, M.F. and Bovik, A.C. (2006) 'A statistical evaluation of recent full reference image quality assessment algorithms', *IEEE Transaction on Image Processing*, Vol. 15, No. 11, pp.3440–3451.

Tambe, R.G., Talbar, S.N. and Chavan, C.S. (2021) 'Satellite image fusion using undecimated rotated wavelet transform', *International Journal of Computational Science and Engineering*, Vol. 24, No. 2, pp.171–184.

Tzannes, A.P. and Mooney, J.M. (1995) 'Measurement of the modulation transfer function of infrared cameras', *Optical Engineering*, Vol. 34, No. 6, pp.1808–1817

Wang, Z., Bovik, A.C., Sheikh, H.R. and Simoncelli, E.P. (2004) 'Image quality assessment: from error visibility to structural similarity', *IEEE Transaction on Image Processing*, Vol. 13, No. 4, pp.600–612.

Wang, Z., Simoncelli, E.P. and Bovik, A.C. (2003) 'Multiscale structural similarity for image quality assessment', *Proceedings of The Thirty-Seventh Asilomar Conference on Signals, Systems & Computers*, IEEE.

Wei, Z.L., Zhu, G.L., Liang, X.Z. and Liu, W.J. (2020) 'An image fusion dehazing algorithm based on dark channel prior and retinex', *International Journal of Computational Science and Engineering*, Vol. 23, No. 2, pp.115–1234.

Williams, D. (1998) 'Benchmarking of the ISO 12233 slanted-edge spatial frequency respons', *Society for Imaging Science and Technology: Image Processing, Image Quality, Image Capture, Systems Conference*, IS&T, pp.17–20.

Xie, X., Fan, H., Wang, H. et al. (2018a) 'Error of the slanted edge method for measuring the modulation transfer function of imaging system', *Applied Optics*, Vol. 57, No. 7, pp.B83–B91.

Xie, X.F., Fan, H.D., Wang, A.D., Zou, N.Y. and Zhang, Y.C. (2018b) 'Regularized slanted-edge method for measuring the modulation transfer function of imaging systems', *Applied Optics*, Vol. 57, No. 22, pp.6552–6558.

Yu, Z.Y., Li, S., Sun, L.J., Liu, L. and Wang, H.N. (2022) 'Multi-distribution noise quantisation: an extreme compression scheme for transformer according to parameter distribution', *Connection Science*, Vol. 34, No. 1, pp.990–1004.

Zhang, H.S., Li, C. and Duan, Y.X. (2018) 'Modified slanted-edge method to measure the modulation transfer function of camera', *Optik*, Vol. 157, pp.635–643.

Zhou, F., Yao, R.G., Liu, B.Z. and Qiu, G.P. (2019) 'Visual quality assessment for super-resolved images: Database and method', *IEEE Transactions on Image Processing*, Vol. 28, No. 7, pp.3528–3541.

Zhou, W. and Chen, Z.B. (2021) 'Deep multi-scale features learning for distorted image quality assessment', *Proceedings – IEEE International Symposium on Circuits and Systems*, IEEE, p.9401285.

Zhou, Z.H., Li, J., Quan, Y.H. and Xu, R.T. (2021) 'Image quality assessment using kernel sparse coding', *IEEE Transactions on Multimedia*, Vol. 23, No. 9113337, pp.1592–1604, IEEE.